


Novel concept for VCSEL enhanced silicon photonic coherent transceiver

Cite as: AIP Advances 9, 105114 (2019); doi: 10.1063/1.5120019

Submitted: 15 July 2019 • Accepted: 9 October 2019 •

Published Online: 18 October 2019



Pascal M. Seiler,^{1,a)} Gregor Ronniger,¹  Ute Troppenz,² Ariane Sigmund,² Martin Moehrle,² Anna Peczek,³ and Lars Zimmermann^{1,4}

AFFILIATIONS

¹Technische Universität Berlin, Institut für HF- und HL-Systemtechnologien, Berlin, Germany

²Fraunhofer Heinrich-Hertz-Institute, Einsteinufer 37, Berlin, Germany

³IHP Solutions, Im Technologiepark 25, Frankfurt (Oder), Germany

⁴IHP, Im Technologiepark 25, Frankfurt (Oder), Germany

^{a)}Electronic mail: seiler@tu-berlin.de

ABSTRACT

We present a novel concept for an integrated silicon photonic coherent transceiver using vertical-emitting laser sources at 1550 nm. In a state of the art external modulation configuration, we deploy a VCSEL on the transmit and a HCSEL on the receive side. We demonstrate the feasibility of this approach by externally modulating the VCSEL with QPSK at up to 28 Gbaud. We also perform experiments with the VCSEL-HCSEL configuration in a slave-master optical injection locking setup for future data center interconnects. The results show stable locking conditions and the VCSEL is detuned to perform predominant phase modulation. To the best of our knowledge, this is the first time direct phase modulation of a VCSEL under optical injection locking was demonstrated using two vertically emitting laser sources as master - and slave laser.

© 2019 Author(s). All article content, except where otherwise noted, is licensed under a Creative Commons Attribution (CC BY) license (<http://creativecommons.org/licenses/by/4.0/>). <https://doi.org/10.1063/1.5120019>

I. INTRODUCTION

Currently, there is an intense debate about how far coherent communication will be deployed for short-reach intra data center interconnects (up to 10 km) in the future, which are presently entirely served by direct detect systems. While for example 850 nm vertical-cavity surface-emitting lasers (VCSELs), which are used for the shortest link distances, have been demonstrated to support data rates >70 Gbps using direct modulation- and detection,¹ the spectral efficiency is limited. Coherent communication generally requires a more complex modulation scheme. However, it also offers a scalable technology, able to support highly spectral efficient modulation formats commonly used for longer link distances. It is therefore a viable approach for supporting the increasing data rate demands of future intra data center interconnects. Silicon photonics has proven to be a high potential technology in the coherent domain.² Silicon photonics also has the scaling capabilities essential for intra data center interconnects. However, there are several economic as well as technical challenges that so far prevented silicon photonics based

short-reach interconnects. Among other issues one needs to consider that 1) narrow linewidth tunable laser sources are a major cost-item in present coherent modules. 2) Silicon photonic modulators show undesirable tradeoffs with respect to insertion loss and power consumption.³ In this paper we would like to discuss some important aspects of a novel concept for the use of mixed laser sources flip-chip integrated with silicon photonics, which would address both issues. The concept goes beyond traditional laser integration that aims at mere light source integration. The basic perceived TROSA (transmitter/receiver optical sub-assembly) structures are depicted in [Figure 1](#). We propose the use of VCSEL and horizontal-cavity surface-emitting DFB laser (HCSEL) sources integrated with a silicon photonics platform such as photonic BiCMOS to enable coherent transmission. The rationale behind the use of VCSEL and HCSEL sources are as follows. Both are vertical emitters and therefore intrinsically compatible with flip-chip soldering on silicon photonic grating couplers,⁴⁻⁶ which is at present a comparatively mature integration technology. In addition, VCSEL technology (in the 850-1000 nm range) has made tremendous

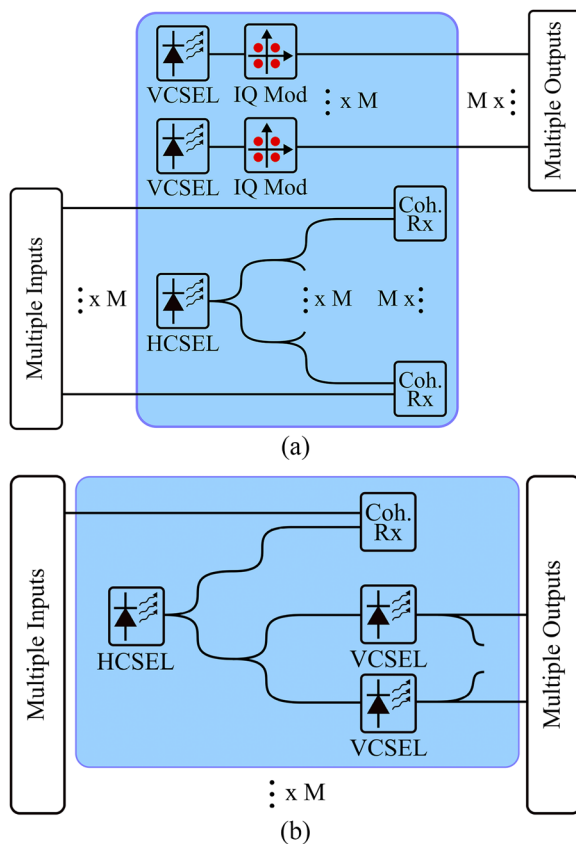


FIG. 1. Concept for an integrated coherent silicon photonics transceiver chip (blue box) using energy efficient and low cost VCSELs and utilizing multiple splitting of a HCSEL. (a) Traditional configuration using external IQ modulators. (b) Optical injection locking using the HCSEL as master and the VCSELs as slaves for direct coherent modulation techniques. IQ Mod: IQ modulator, Coh. Rx: coherent receiver.

progress, with volume applications of VCSELs now being in the consumer market, demonstrating that VCSELs have the potential to be very low cost.⁴ HCSELs on the other hand show considerably higher output power and smaller linewidth than VCSELs. Combining HCSELs and VCSELs therefore has the potential to provide more cost-effective solutions than HCSEL-only solutions, fulfilling at the same time basic optical power requirements, especially on the receive side. The 2nd important aspect is that VCSELs have the potential to bypass the external silicon photonic modulator. Omitting the silicon photonic modulator could lead to considerable savings of chip-footprint and power. To this end we propose the use of optical injection locking of VCSELs for phase modulation, which can effectively detune a laser to work in a regime of predominant phase response under direct modulation. VCSELs have shown to be compatible with coherent communication^{7–10} and the injection locking of VCSELs in particular has been under investigation in recent years.^{11–15} Optical injection is also known to be able to enhance the relaxation oscillation frequency, bandwidth and reduce relative intensity noise.¹⁶ Despite of these advantages,

there are clear drawbacks of VCSELs as well, in particular their limited output power. Further concerns arise, due to their generally larger linewidth in comparison to edge-emitters. Both issues can be addressed by deploying a vertically emitting DFB laser in combination with VCSELs.

In this article, we study experimentally for the first time important aspects of this novel concept for coherent transceiver based on two different surface-emitting lasers. First, we shall demonstrate the operation of this configuration in a 56 Gbps experiment deploying external modulation. A VCSEL is used at the transmitter and a HCSEL at the receiver, acting as local oscillator. The VCSEL will be modulated with quadrature-phase shift-keying (QPSK) at up to 28 Gbaud. Following, we investigate the combination of VCSEL and HCSEL for future integrated coherent interconnects using optical injection locking, bypassing the need for external modulators. A VCSEL will be locked to an external-cavity laser (ECL) and amplitude responses will be measured as a reference. Subsequent, the VCSEL will be locked to the HCSEL and amplitude responses, as well as coherent large-signal modulation measurements will be performed. The operation of the VCSEL in a regime of predominant phase modulation will be investigated. In the external modulation configuration, the transmitter benefits from the low power consumption and the small footprint of VCSEL structures. The receiver profits from the higher output power of the DFB laser (see Fig. 1 (a)). The integration of the power efficient VCSEL and the high output power HCSEL also offers the employment of more flexible and novel concepts, like optical injection locking (see Fig. 1 (b)). Depending on the application, the VCSELs locked to the HCSEL can be tuned to regimes of phase modulation and directly modulated. Integrated solution could also include interferometric structures to remove remaining chirp. This way, coherent modulation formats like QPSK can be achieved without the use of external IQ modulators.^{14,15} Due to the co-integration of a high power surface emitting laser, this concept of only surface emitting lasers offers the possibility of cost efficient flip-chip bonding in the TROSA. These potential advantages are particularly important for fully monolithic integration platforms, such as photonic BiCMOS.¹⁷

II. EXTERNAL MODULATION EXPERIMENT

This section will first provide information concerning the used laser devices and their determined intrinsic linewidths. Following, the employed back-to-back measurement setup will be discussed. Finally, the applied offline processing is described and the results presented.

A. Device characteristics

The VCSEL used in this work is an unpackaged single mode VCSEL with an integrated buried tunnel junction (BTJ) and manufactured by VERTILAS. At a temperature of 20 °C, it is operating at an emission wavelength around 1550 nm, with a threshold current of 1.77 mA and a maximal output power of about 1.89 mW. A power-current-voltage (P-I-V) characteristic of the structure is given in Figure 2 (a). The minimal intrinsic linewidth of similar structures of the same manufacturer have been found to be around 6-7 MHz using a delayed self-heterodyne measurement setup, employing an acousto-optic modulator and a 20 km delay-line.

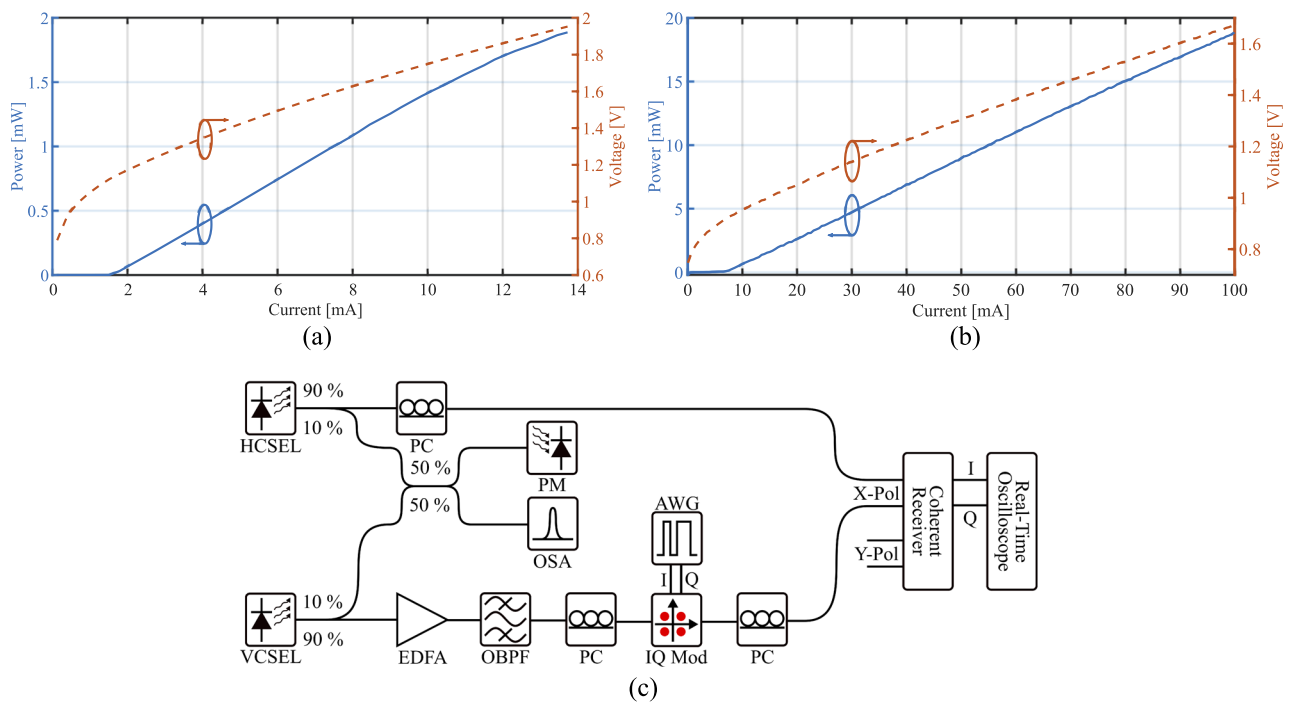


FIG. 2. Power-current-voltage characteristic at a temperature of 20 °C of (a) a 1550 nm BTJ single mode VCSEL (b) a 1550 nm single mode HCSEL. (c) Experimental setup for external modulation of a VCSEL at the transmitter and a HCSEL at the receiver as local oscillator. A QPSK is externally applied to the VCSEL carrier using an IQ modulator (IQ Mod) and arbitrary waveform generator (AWG). PC: polarization controller, OSA: optical spectrum analyzer, OBPf: optical bandpass filter, IQ Mod: IQ modulator, EDFA: erbium-doped fiber amplifier, X/Y-Pol: x/y-polarization input, PM: power meter.

The intrinsic linewidth has been determined by applying a Voigt-fitting on the recorded electrical spectrum. The C-band HCSEL is based on a buried hetero structure with complex-coupled DFB-grating. The device comprises an absorber section at the rear side that allows the monitoring of the optical power.^{18,19} In this experiment, a new HCSEL design suited for flip-chip integration is used. Furthermore, an active taper section in front of the DFB part provides increased optical power and a symmetrical beam profile with a typical full-width half-maximum far field angle $\leq 20^\circ$. The 380 μm long HCSEL chip includes a 100 μm long active taper section. A P-I-V characteristic at a temperature of 20 °C is shown in Fig. 2 (b). The etched front facet enables an outcoupled beam propagation with $\approx 10^\circ$ perpendicular to the chip surface, which matches well to coupling angles typically used in silicon-based grating couplers. The intrinsic linewidth of these HCSEL structures has been determined with a delayed self-homodyne measurement setup and further extraction of the Lorentzian part, as well as by measuring the phase noise spectra. Both methods reveal a typical intrinsic linewidth < 500 kHz.

B. Experimental setup

The measurement setup used in this section is illustrated in Fig. 2 (c). The VCSEL and HCSEL are placed on thermally independent controlled stages and manually coupled via lensed fibers. The

VCSEL is thermally stabilized at 20.3 °C and biased with 11 mA, which results in -2.5 dBm optical output power. The HCSEL is biased at 90 mA with an output power of +8.5 dBm. This indicates an increased coupling loss due to suboptimal fiber coupling using the lensed fiber (see Fig. 2 (b)). The temperature of the HCSEL is tuned to match its emission wavelength to that of the VCSEL, which is around 1549 nm. Both signals are connected to 10 dB couplers for further monitoring of the chip-to-fiber coupling and the optical spectra. While observing the optical spectrum analyzer (OSA, Advantest Q8384), the wavelength drift between the two lasers is found to be well below 0.1 nm (OSA resolution 0.01 nm). The VCSEL signal is then amplified to +17 dBm using an erbium-doped fiber amplifier (EDFA) to compensate for the following IQ modulator's (ID Photonics OMFT) insertion loss. The amplified signal is subsequently optically filtered with a 1 nm bandwidth optical bandpass filter. The optical modulator is supplied with two 700 mVpp, non-return-to-zero (NRZ) coded, 2^9-1 pseudo-random binary sequences (PRBS) by an arbitrary waveform generator (AWG, Keysight M8195A), with one electrical signal being delayed by 256 bits. The AWG has a bandwidth of 22 GHz and is operating at 65 GSa/s. Raised cosine filters ($\alpha=1$ for 10 and 20 Gbaud, $\alpha=0.5$ for 28 Gbaud) are employed internally by the AWG. Baudrates of 10, 20 and 28 Gbaud are supplied to the modulator. The VCSEL and HCSELs are respectively manually polarization-controlled to match the coherent receiver's x-polarization input

(Fraunhofer HHI CRF-70-EH). The local oscillator's (HCSEL) and the modulated VCSEL's average optical power at the receiver are +7 dBm and -1.7 dBm, respectively. Further optimizing the optical coupling to the HCSEL would potentially allow for an increased power budget for additional link distance and/or on-chip splitting. The electrical signals are then sampled by two real-time oscilloscopes (Tektronix DPO77002SX), operating at 200 GSa/s. The bandwidth of the two oscilloscope channels are adjusted for each baudrate (26 GHz and 33 GHz for 10 Gbaud and 20/28 Gbaud, respectively) to reduce the signal-to-noise ratio degradation due to shot noise. The bandwidth for the 28 Gbaud recording was reduced to 26 GHz in the offline processing. Segments of 8 million samples are recorded for each channel and stored for further offline processing.

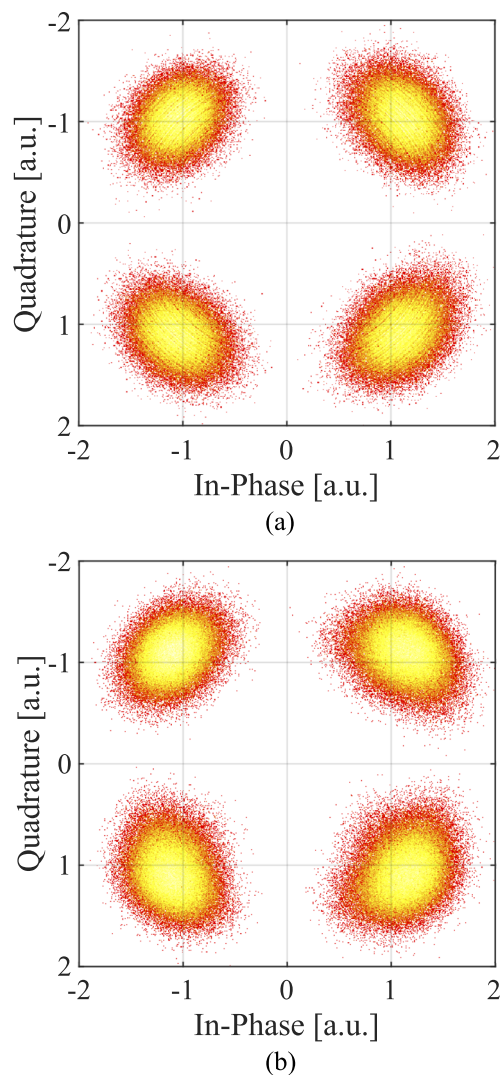


FIG. 3. Recovered QPSK constellation employing an externally modulated VCSEL-HCSEL configuration at (a) 20 Gbaud (b) 28 Gbaud.

C. Offline processing and results

All offline processing is done with MATLAB. Existing DC-offsets are first subtracted and the data is then normalized by dividing by its root-mean-square. Following, the frequency offset due to the beating between the VCSEL's and HCSEL's optical fields is compensated by a 4-th power, FFT-based coarse frequency estimator using MATLAB's communication toolbox functions. The data stream is then resampled to the symbol rate and fed to a second order decision-directed phase-locked-loop (DD-PLL) as presented in Refs. 8, 20, and 21. The DD-PLL is tuned for each baudrate for a minimal bit error-rate (BER). For the BER calculation, the first 1k symbols are omitted to guarantee that the phase recovery loop is locked. The resulting recovered constellation for a data rate of 20 Gbaud and 28 Gbaud is shown in Fig. 3 (a) and (b), respectively. The data is plotted as a 2D histogram in a logarithmic colorscale. We find error-free transmission for 10, 20 and 28 Gbaud over the observed segment of 400k symbols, resulting in a BER below $1.25 \cdot 10^{-6}$. This error rate is similar to that of other groups that implement one or more high phase noise lasers in back-to-back setups.^{7,8} However, in this work we demonstrated a novel configuration, consisting of a VCSEL as a high phase noise laser and a HCSEL as an intermediate phase noise laser (linewidth <500 kHz), compared to traditional DFB lasers. The results show, that the proposed configuration of two surface-emitting lasers is able to provide state of the art performance in an external modulation setup.

III. OPTICAL INJECTION LOCKING EXPERIMENT

This section will investigate the feasibility of the VCSEL-HCSEL approach in an optical injection locking configuration for future coherent short-reach datacenter interconnects. First, a VCSEL is locked to an ECL at different external injection ratios R_{inj} , defined as the ratio of input power from the master laser power and free running output power of the slave laser. The VCSEL will then be injection locked to the HCSEL, acting as the master laser. The HCSEL's wavelength is thermally tuned to drive the VCSEL in different operating points and the amplitude- and phase modulation is investigated.

A. VCSEL-ECL optical injection locking

We first lock a VCSEL to an ECL to determine the dependency of the VCSEL's response on the external injection ratio. For this, the setup in Figure 4 is used. The VCSEL is biased at 4.2 mA with approximately -3 dBm optical output power under nearly vertical coupling with a lensed fiber. The DC signal is combined with a sine supplied by an RF source (Keysight E8257D) using a 45 GHz bias-tee. The VCSEL is kept at 25 °C. The ECL is amplified to 20 dBm output power and subsequently attenuated. This allows to maintain external injection ratios of 5, 10 and 20 dB with minimal change to the setup between the measurements. The ECL is polarization-controlled to match the VCSEL's polarization. VCSEL and ECL are connected via a circulator, whose output is connected to a 20 dB coupler. The low power path is used for monitoring the VCSEL coupling and the high power path is connected to an electrical spectrum analyser (ESA, FSUP50). For the large-signal measurement, RF source and ESA are exchanged for a bit-pattern

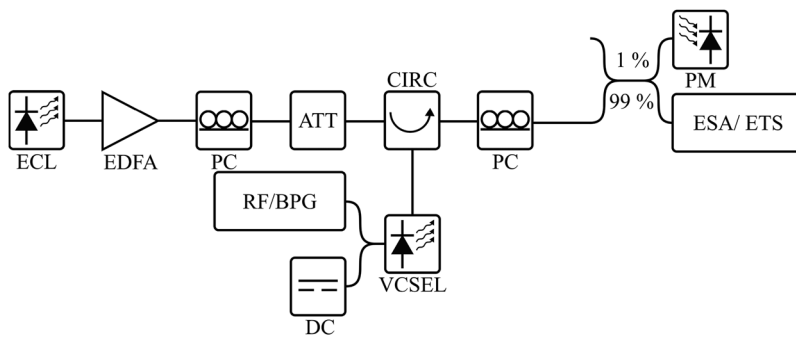


FIG. 4. Experimental optical injection locking setup with a 1550 nm single mode VCSEL as slave laser and an ECL as master laser. The ECL is amplified using an EDFA with subsequent attenuation (ATT) to set different injection ratios. BPG: bit pattern generator, PM: power meter, PC: polarization controller, CIRC: circulator, ESA: electrical spectrum analyzer, ETS: Equivalent-time oscilloscope.

generator (BPG, Sympuls Aachen BMG 2500) and an equivalent-time oscilloscope (ETS, Agilent DCA-X 86100D). The ECL is swepted in its emission wavelength and at each detuning the VCSEL's amplitude response is measured using the ESA at a modulation power of -20 dBm. Responses at various wavelength detunings for 5 and 10 dB injection ratio are shown in Figure 5 (a) and (b), respectively. A core difference between the behavior for both injection ratios is an increased locking range for increasing injection ratios, which is due to the higher optical power injected in the VCSEL cavity.¹⁶ For negative detunings, we find an enhanced relaxation oscillation frequency, which is roughly proportional to $\sqrt{R_{inj}}$ in our measurements. This is in agreement with the expected behavior. The enhancement originates from the beating between the master laser frequency and the slaves natural cavity frequency, which is red-shifted compared to the free running frequency. Therefore, a maximal relaxation oscillation frequency enhancement can

be found at the negative edge of the locking range.¹⁶ We also find that for an increasing wavelength detuning, the VCSEL transitions from a moderate low-frequency amplitude response (see Fig. 5 (b), $\Delta\lambda = -124$ pm) to a low-frequency amplitude suppression ($\Delta\lambda = +200$ pm). Further increasing the wavelength detuning changes the VCSEL's amplitude response to low-frequency amplitude gain ($\Delta\lambda = +600$ pm). The low-frequency gain is again caused by the beating between the master laser and the red-shifted natural cavity frequency.^{13,16} The low-frequency suppression point is associated with a minimal amplitude response of the device under direct modulation and also a point of pattern inversion.^{12,13} We verify the pattern inversion at an injection ratio of 20 dB using a pattern generator operating at 1 Gbaud with an amplitude of 470 mVpp and a sampling oscilloscope. The results are shown in Figure 6. It shows, that the VCSEL performs a pattern inversion by transitioning over the amplitude modulation suppression point, which in this case was in a detuning window of $\Delta\lambda \in [220, 320]$ pm.

In this section, we investigated the optical injection locking of a 1550 nm single mode VCSEL to an ECL as a master laser. Different injection ratios were set and the VCSEL's amplitude response at various wavelength detunings was measured. The characteristics include points of increased resonance frequencies, low-frequency amplitude suppression and low-frequency amplitude gain. The edges of the locking range, associated with the enhanced resonance frequency and the low-frequency gain, are depending on the injection ratio.^{12,13,16} The required detuning for the low-frequency amplitude suppression increased only slightly by increasing the injection ratio

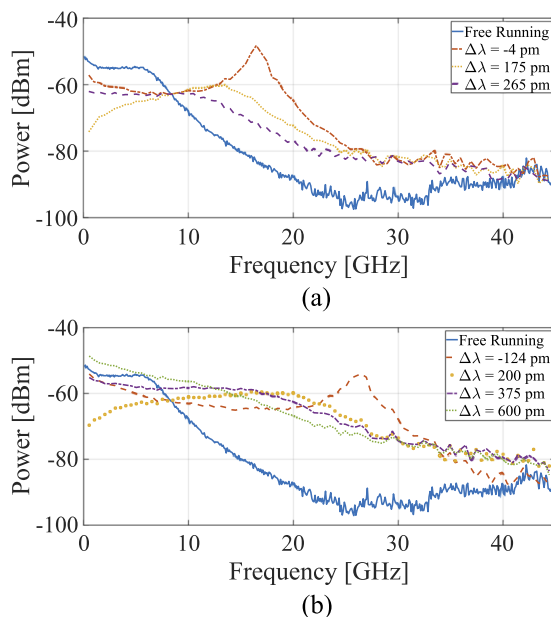


FIG. 5. Amplitude response of a VCSEL under optical injection locking to an ECL master at (a) 5 dB and (b) 10 dB injection ratio. The free running 3 dB bandwidth of the VCSEL is approximately 7 GHz.

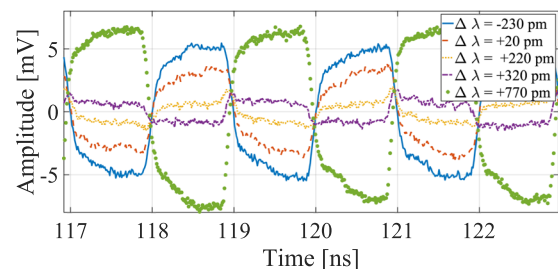


FIG. 6. Directly modulated VCSEL locked to an ECL under 20 dB injection ratio at 1 Gbaud. The VCSEL transitions from moderate low-frequency modulation ($\Delta\lambda = -230$ pm) to low-frequency suppression ($\Delta\lambda = +220$ pm). Further increasing the wavelength detuning causes a pattern inversion and for larger detunings a low-frequency gain ($\Delta\lambda = +770$ pm).

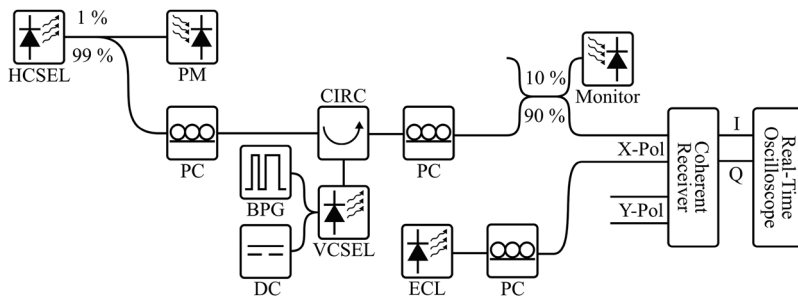


FIG. 7. Experimental setup for direct phase modulation using a VCSEL as slave laser and a HCSEL as master laser. An external-cavity laser (ECL) is used as local oscillator. A 10 Gbaud PAM-2 signal is directly applied to the VCSEL using a bit pattern generator (BPG). The monitoring path of the VCSEL also includes an optical - and an electrical spectrum analyzer. PM: power meter, PC: polarization controller, CIRC: circulator, X/Y-Pol: x/y-polarization input.

compared to the increase in locking range. The results indicate this behavior in a detuning range of $\Delta\lambda \in [175, 320]$ pm.

B. VCSEL-HCSEL optical injection locking

This section will investigate the feasibility of the proposed VCSEL-HCSEL configuration for future datacom interconnects employing injection locking applications, such as direct phase modulation. Therefore, the characteristic behavior determined in the prior section will be analyzed and the phase - and amplitude modulation will be measured using a coherent measurement setup.

1. Experimental setup

The setup for the optical injection locking of a VCSEL to the HCSEL is given in Figure 7. The VCSEL in this experiment is kept at a constant temperature of 20.2 °C. It is biased at 6 mA with an optical output power of approximately -1.2 dBm. The HCSEL is identical to the prior QPSK experiment and biased at 80 mA with an output power of +8 dBm, resulting in an injection ratio of 7 dB due to splitting and connector losses. Both lasers are coupled via lensed fibers and the VCSEL is coupled nearly vertical to the chip surface. The temperature of the HCSEL is tuned between 30 °C and 34 °C during the measurement to achieve different detunings at the slave laser.

The HCSEL is first connected to a 20 dB coupler, with the low power arm used for monitoring of the coupling. The other arm is polarization controlled to match the polarization of the VCSEL, which is connected to the HCSEL via a circulator. The VCSEL is supplied with a 550 mVpp, 10 Gbaud 2^9-1 PRBS, NRZ coded signal from a pattern generator (BPG, Sympuls Aachen BPG 4x32G) and combined with the DC bias via a bias-tee with 67 GHz bandwidth. It should be noted that the RF connection from the pattern generator to the VCSEL requires a long RF cable connection, which significantly distorts the RF signal and causes unwanted loss, reducing the voltage swing. The circulator output is connected to a 10 dB coupler, with the low power path used for monitoring. The monitoring of the VCSEL also includes an OSA (identical to the prior experiment) and an electrical spectrum analyzer (ESA, PXA N9030A). Finally, the signal is connected to the same coherent receiver and real-time oscilloscope as in the prior experiment, operating in this experiment at 100 Gsa/s and a bandwidth of 20 GHz. An ECL with an output power of +15 dBm is used as local oscillator in this setup. The emission wavelength of the ECL is tuned to the locked VCSEL during the measurement. Segments of 40 thousand samples are recorded for each channel and stored for further offline processing. For the response measurements, the pattern generator is exchanged with a RF generator (Anritsu MG 3697C).

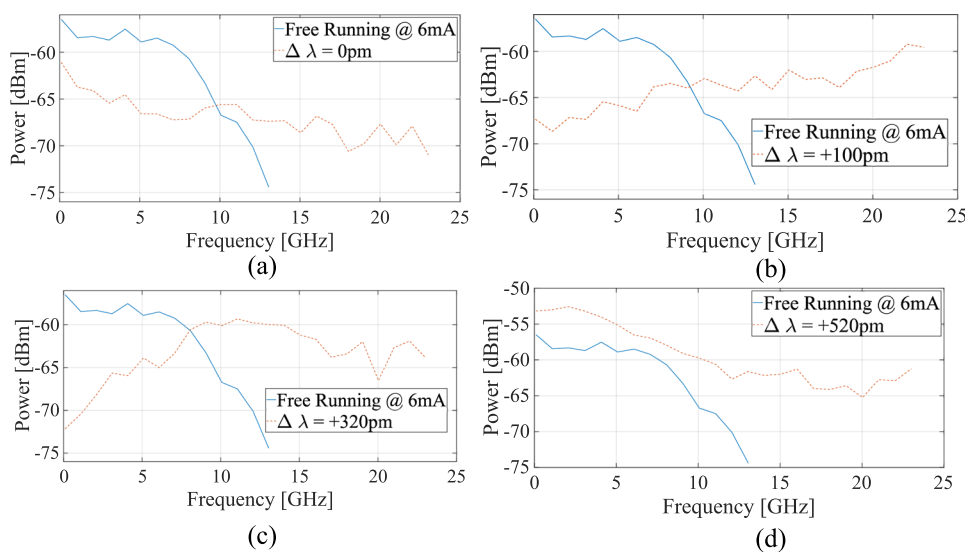


FIG. 8. Small-signal amplitude response of a 1550 nm VCSEL under optical injection locking to a HCSEL as master at an injection ratio of 7 dB. The VCSEL is detuned to approximately (a) $\Delta\lambda = 0$ pm (b) $\Delta\lambda = +100$ pm (c) $\Delta\lambda = +320$ pm (d) $\Delta\lambda = +520$ pm.

2. Results

First, the characteristic behavior from the VCSEL-ECL injection locking will be reproduced to determine whether stable locking conditions can be maintained. Therefore, the pattern generator is exchanged for a sine generator and the VCSEL is directly modulated with a RF power of -10 dBm. The HCSEL is thermally tuned to different emission wavelengths, which detunes the VCSEL at a constant injection ratio of 7 dB. At various detunings, amplitude response measurements are performed. The aforementioned electrical path loss is measured using an ESA and accounted for in offline processing for the response measurements. The results are presented in Figure 8. Detuning the VCSEL from around 0 pm to +100 pm

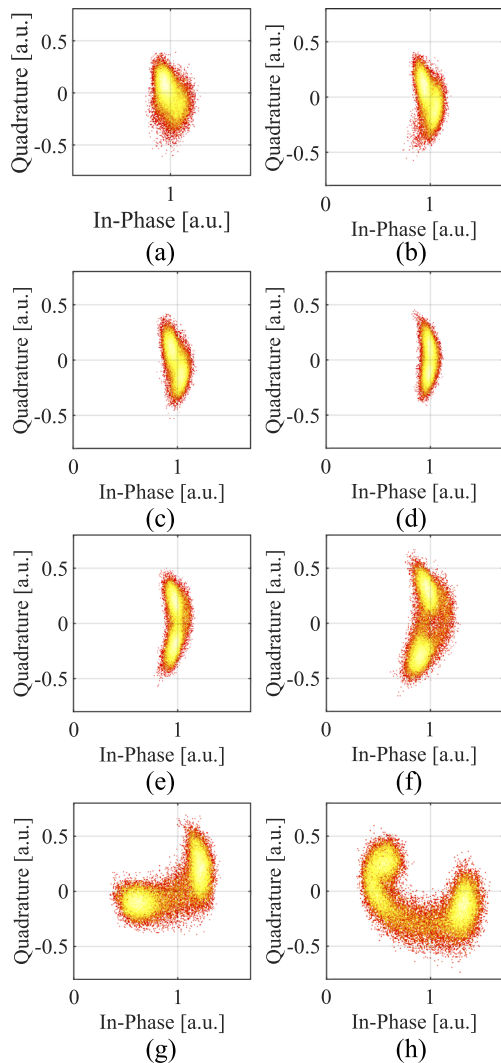


FIG. 9. Recovered constellations at 10 Gbaud of a directly modulated VCSEL optical injection locked to a HCSEL at an injection ratio of 7 dB. The HCSEL is tuned to achieve wavelength detunings of approximately (a) $\Delta\lambda = 0$ pm (b) $\Delta\lambda = +130$ pm (c) $\Delta\lambda = +180$ pm (d) $\Delta\lambda = +230$ pm (e) $\Delta\lambda = +296$ pm (f) $\Delta\lambda = +358$ pm (g) $\Delta\lambda = +600$ pm (h) $\Delta\lambda = +638$ pm.

(compare Fig. 8 (a) and (b), respectively) shows a transition from a moderate low-frequency amplitude response to a reduced low-frequency response. Further increasing the detuning to + 320 pm (Figure 8 (c)) indicates the transition point of suppressed low-frequency amplitude response. Significantly increasing the wavelength detuning to $\Delta\lambda = +520$ pm (Figure 8 (d)) tunes the VCSEL to respond with an increased low-frequency amplitude gain. We find good agreement between the VCSEL-ECL reference measurement and the proposed VCSEL-HCSEL configuration. This indicates that this configuration can produce and maintain stable injection locking operation. This is further investigated by large-signal modulation of the VCSEL at different wavelength detunings with the coherent detection setup. The constellation diagrams of various detunings at an injection ratio of 7 dB are shown in Figure 9 as 2D histograms in a logarithmic colorscale. The data is normalized by dividing it by its root-mean-square and the frequency offset from the heterodyne beating of the locked VCSEL and the ECL is compensated for. The data is also rotated to be positioned around 0 rad. Beginning at a detuning of approximately $\Delta\lambda = 0$ pm, the VCSEL shows no significant phase or amplitude modulation (comp. Fig. 9 (a)). Further increasing the wavelength detuning transitions the VCSEL in the phase modulation regime, as was indicated by the response measurements (see Fig. 9 (b) to (d)). For detunings between $\Delta\lambda = +296$ pm and $\Delta\lambda = +358$ pm the VCSEL shows a minimal amplitude modulation while operating in a predominant phase modulation regime (see Fig. 9 (e) and (f)). The phase modulation in this regime is determined to be around 35 to 40°. Further increasing the wavelength detuning drives the VCSEL in a regime of increased low-frequency amplitude gain (comp. Figure 9 (g) and (h)). The predominant phase modulation changes in this domain to amplitude modulation. This can be explained by assuming that part of the HCSEL signal is reflected at the VCSEL's mirror and is then interfering with the locked VCSEL signal causing a complex offset.¹³ While this is working towards the phase modulation for smaller detunings, we find it to be the cause of a unwanted shift in the complex offset and thus the amplitude modulation for increasingly higher detunings. We verify the results by increasing the injection ratio. The VCSEL is now biased at 4.5 mA and the HCSEL at 100 mA, resulting in an optical output power of -3 dBm and +9 dBm, respectively. The injection ratio is approximately 10 dB. The VCSEL is tuned to a point of low-frequency amplitude suppression and low-frequency amplitude gain. Large-signal measurements were performed at each detuning and the results are

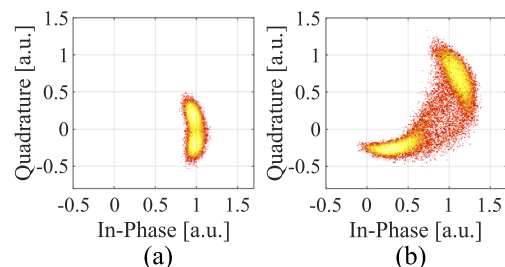


FIG. 10. Recovered constellations at 10 Gbaud of a directly modulated VCSEL optical injection locked to a HCSEL at an injection ratio of 10 dB. The HCSEL is tuned to achieve wavelength detunings of approximately (a) $\Delta\lambda = +300$ pm (b) $\Delta\lambda = +880$ pm.

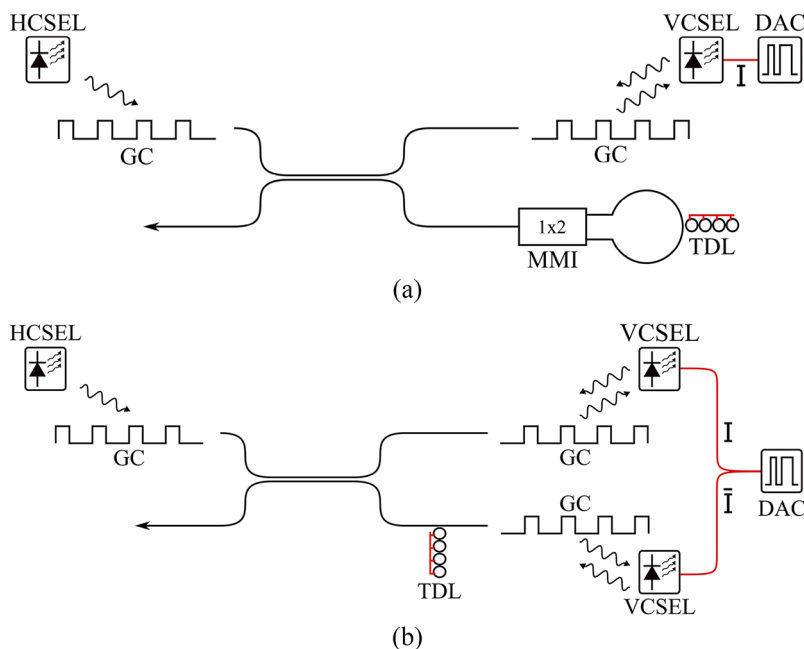


FIG. 11. Concept for an integrated coherent transmitter using a VCSEL-HCSEL approach. (a) A part of the HCSEL is split for interference with the locked VCSEL to adjust the complex offset. (b) A second VCSEL is modulated with the inverse pattern to interfere with. This removes the complex offset and creates chirp-free modulation.¹⁴ The red lines indicate electrical connections. GC: grating coupler, TDL: tunable delay-line, MMI: multi-mode interferometer.

given in Figure 10. The results for 10 dB injection ratio show a similar behavior and phase swing at the low-frequency amplitude suppression point.

3. Discussion

We measured a phase swing of approximately 35 to 40° at a detuning for minimal amplitude modulation. Further increasing the detuning did not increase the phase modulation, but presumably changed the interference of reflected master and slave field. This moves the phase modulation to a state of amplitude modulation. However, the maximal achievable phase modulation in this experiment might be limited due to the aforementioned poor RF connection to the VCSEL, which reduces the modulation swing. Another group achieved under similar locking condition with VCSELs of the same manufacturer a maximal phase modulation of around 100° (see Ref. 14) at 470 mVpp, which indicates that the modulation voltage might be the cause of the limited phase modulation. Even with a limited phase modulation, there are possible approaches to this problem. We reported the existence of a complex offset at the positive locking edge, which can presumably only be found using heterodyne detection. Using a homodyne detection scheme by splitting the HCSEL, the interference of the local oscillator and the signal field could effectively suppress this unwanted complex offset. Similar, in an integrated solution, this could be achieved by interfering a VCSEL driven at the positive edge (see Fig. 10 (b)) with a split portion of the master laser. The relative phase of the two signals needs to be adjusted for that purpose. A schematic of this concept is given in Figure 11 (a). After splitting the HCSEL signal using a directional coupler, the light could be reflected using a 1x2 multi-mode interferometer (MMI) and a tunable delay-line (TDL). The TDL is conceptualized using silicon photonic ring resonators. Another solution was proposed by using two VCSELs in a push-pull configuration.¹⁴ This would create a chirp-free modulation and would

remove the complex offset we reported on in this work. A schematic is shown in Figure 11 (b). In both cases, an interferometric structure required for this is readily available in silicon photonics. Using two VCSELs operating within a regime of predominant amplitude modulation could also be an effective way to produce i.e. QPSK by creating a 90° offset between two directly modulated VCSELs.¹⁵ Splitting the HCSEL for the use of multiple VCSELs for QPSK using the proposed concept is plausible, since we performed the locking at 7 dB and 10 dB, indicating a sufficient power budget. In general, an injection ratio greater than 5 dB is required for these applications.¹⁴

In this section, we demonstrated the proposed novel concept of two surface-emitting lasers for optical injection locking applications in silicon photonics. We verified the behavior compared to a reference measurement using a VCSEL as slave and an ECL as master laser. We found an operating point of predominant phase modulation, as indicated by the response measurements. For increasing detunings, we reported on a complex offset due to the interference of the master laser reflection and the locked slave signal. We also discussed possible solutions, which are readily available in silicon photonics.

IV. CONCLUSION

The content presented in this work is two-fold. First, we proposed a novel concept for integrated coherent transceiver for data center interconnects. The use of a power efficient VCSEL and a high power HCSEL allows for the power budget necessary in coherent communication, while maintaining the possibility of cost efficient flip-chip bonding of both devices. We demonstrated the feasibility of this approach in a state of the art 56 Gbps QPSK experiment employing an external IQ modulator. Second, we thoroughly investigated the optical injection locking of the HCSEL as master laser

to the VCSEL as slave laser. We achieved operating points of predominant phase modulation under direct modulation, bypassing the need for external modulation. To the best of our knowledge, this is the first time direct phase modulation of a VCSEL under optical injection locking was demonstrated using two vertically-emitting laser sources as master - and slave laser. We also reported on a complex offset on the positive edge of the locking range and discussed solutions to adjust to this offset. These solutions are straightforward to implement in silicon photonics. This indicates that novel integration concepts, such as the one presented in this work, could become a powerful extension of current silicon photonic optical interconnect solutions. When integrated, this system has the potential to profit from the low power consumption of the VCSEL and the higher output power and smaller linewidth of the HCSEL, while allowing for cost efficient and low footprint flip-chip bonding in the TROSA.

ACKNOWLEDGMENTS

The authors would like to thank VERTILAS GmbH, Munich, Germany, for providing the VCSELs. This work was partially supported by the Deutsche Forschungsgemeinschaft (DFG) through the projects Sopa2 (PE 319/36-2), EPIC-Sense (ZI 1283-6-1) and CRC787, as well as the Bundesministerium für Bildung und Forschung (BMBF) through project SPEED.

REFERENCES

- ¹D. M. Kuchta, A. V. Rylyakov, F. E. Doany, C. L. Schow, J. E. Proesel, C. W. Baks, P. Westbergh, J. S. Gustavsson, and A. Larsson, *IEEE Photon. Technol. Lett.* **27**, 577 (2015).
- ²C. Doerr and L. Chen, *Proceedings of the IEEE* **106**, 2291 (2018).
- ³D. Petousi, L. Zimmermann, A. Gajda, M. Kroh, K. Voigt, G. Winzer, B. Tillack, and K. Petermann, *IEEE J. Sel. Topics Quantum Electron.* **21**, 199 (2015).
- ⁴A. Liu, P. Wolf, J. A. Lott, and D. Bimberg, *Photon. Res.* **7**, 121 (2019).
- ⁵H. Lu, J. S. Lee, Y. Zhao, C. Scarcella, P. Cardile, A. Daly, M. Ortsiefer, L. Carroll, and P. O'Brien, *Opt. Express* **24**, 16258 (2006).
- ⁶K. Kaur, A. Subramanian, P. Cardile, R. Verplancke, J. V. Kerrebrouck, S. Spiga, R. Meyer, J. Bauwelinck, R. Baets, and G. V. Steenberge, *Opt. Express* **23**, 28264 (2015).
- ⁷G. Meloni, A. Malacarne, F. Fresi, and L. Poti, "6.27 bit/s/hz spectral efficiency VCSEL-based coherent communication over 800km of SMF," in *2015 Optical Fiber Communications Conference and Exhibition (OFC)* (2015).
- ⁸T. N. Huynh, V. Vujicic, M. D. Gutiérrez Pascual, P. M. Anandarajah, and L. P. Barry, "Digital coherent communications with a 1550 nm VCSEL," in *2015 Optical Fiber Communications Conference and Exhibition (OFC)* (2015).
- ⁹S. Kim, N. Sakurai, H. Kimura, and H. Hadama, "VCSEL-based coherent detection of 10-Gbit/s QPSK signals using digital phase noise cancellation for future optical access systems," in *2010 Conference on Optical Fiber Communication (OFC/NFOEC), Collocated National Fiber Optic Engineers Conference* (2010).
- ¹⁰X. Zhang, X. Pang, L. Deng, D. Zibar, I. T. Monroy, and R. Younce, *Opt. Express* **20**, 19990 (2012).
- ¹¹P. Guo, W. Yang, D. Parekh, C. Hong, C. Zhang, Z. Chen, and C. J. Chang-Hasnain, "MPSK modulation by optical injection locked VCSEL," in *Conference on Lasers and Electro-Optics 2010* (2010).
- ¹²P. Guo, T. Sun, W. Yang, D. Parekh, C. Zhang, X. Xie, C. J. Chang-Hasnain, A. Xu, and Z. Chen, *Opt. Express* **21**, 22114 (2013).
- ¹³W. Yang, P. Guo, D. Parekh, and C. J. Chang-Hasnain, *Opt. Express* **18**, 20887 (2010).
- ¹⁴N. K. Fontaine, X. Xiao, H. Chen, B. Huang, D. T. Neilson, K. W. Kim, J. H. Sinsky, R. R. Ryf, G. Raybon, P. Winzer, A. Daly, C. Neumeyr, and M. Ortsiefer, "Chirp-free modulator using injection locked VCSEL phase array," in *ECOC 2016 - Post Deadline Paper; 42nd European Conference on Optical Communication* (2016).
- ¹⁵X. Xiao, N. K. Fontaine, H. Chen, B. Huang, D. T. Neilson, K. W. Kim, J. H. Sinsky, R. R. Ryf, G. Raybon, P. Winzer, A. Daly, C. Neumeyr, M. Ortsiefer, and S. J. B. Yoo, "High-speed IQ modulator based on injection-locked VCSEL array," in *2017 Conference on Lasers and Electro-Optics (CLEO)* (2017).
- ¹⁶E. K. Lau, L. J. Wong, and M. C. Wu, *IEEE J. Sel. Topics Quantum Electron.* **15**, 618 (2009).
- ¹⁷G. Winzer, M. Kroh, S. Lischke, D. Knoll, K. Voigt, H. Tian, C. Mai, D. Petousi, D. Micusik, L. Zimmermann, B. Tillack, and K. Petermann, "Monolithic photonic-electronic QPSK receiver for 28gbaud," in *2015 Optical Fiber Communications Conference and Exhibition (OFC)* (2015).
- ¹⁸F. Heinrich-Hertz-Institute, "Surface-emitting DFB laser arrays," <https://www.hhi.fraunhofer.de/fileadmin/PDF/PC/LAS/20181009-Surface-Emitting-DFB-Laser-Arrays-web.pdf>, accessed 15 April 2019.
- ¹⁹M. Billah, T. Hoose, T. Onanuga, N. Lindenmann, P. Dietrich, T. Wingert, M. Goedecke, A. Hofmann, U. Troppenz, M. Moehrle, A. Sigmund, W. Freude, and C. Koos, "Multi-chip integration of lasers and silicon photonics by photonic wire bonding," in *2015 Conference on Lasers and Electro-Optics (CLEO)* (2015).
- ²⁰T. N. Huynh, A. T. Nguyen, W. Ng, L. Nguyen, L. A. Rusch, and L. P. Barry, *J. Lightw. Technol.* **32**, 1973 (2014).
- ²¹T. N. Huynh, W. Ng, A. T. Nguyen, L. Nguyen, L. A. Rusch, and L. P. Barry, "Tracking excess noise from a monolithic tunable laser in coherent communication systems," in *2013 Optical Fiber Communication Conference and Exposition and the National Fiber Optic Engineers Conference (OFC/NFOEC)* (2013).